Research Article | Vol. 27, No. 24 / 25 November 2019 / Optics Express 34876

Optics EXPRESS

Paper-like flexible optically isotropic liquid crystal film for tunable diffractive devices

RAMESH MANDA,[1,5] JEONG HWAN YOON,[2,5] SRINIVAS PAGIDI,[1] SURJYA SARATHI BHATTACHARYYA,[3] DUNG THI THUY TRAN,[1] YOUNG JIN LIM,[1] JAE-MIN MYOUNG,[2,4] AND SEUNG HEE LEE[1,*]

[1]*Applied Materials Institute for BIN Convergence, Department of BIN Convergence Technology and Department of Polymer Nano Science and Technology, Jeonbuk National University, Jeonju, Jeonbuk, 54896, South Korea*
[2]*Department of Materials Science and Engineering, Yonsei University, Seoul 03722, South Korea*
[3]*Department of Physics, Asutosh College, 92, Shyamaprasad Mukherjee Road, Kolkata 700 026, West Bengal, India*
[4]*jmmyoung@yonsei.ac.kr*
[5]*These authors are equally contributed*
[*]*lsh1@chonbuk.ac.kr*

Abstract: We have demonstrated a paper-like diffractive film in which nano-structured liquid crystal droplets are embedded in elastomeric monomer incorporated polymer matrix by polymerization induced phase-separation. The film with voltage-tunable phase grating exhibits an optically isotropic phase with high transparency and an effective chromatic diffraction for an incident white light with sub-millisecond switching time. In addition, the proposed diffractive film is exhibiting excellent chemical stability against organic and inorganic solvents. In this paper, the diffraction properties of test films depending on incident polarization direction, wavelength, and spatial dispersion are characterized. Easy processing and optically isotropic nature of the film imparts potential applications to flexible electro-optic devices that can be widely implemented in wearable photonics.

1. Introduction

The liquid crystal (LC) devices exhibit several promising applications owing to fascinating properties of end products such as planar shape, compact size, mechanically non-moving parts, low driving field, and lightweight etc. For instance, advantages of LC have been utilized to fabricate non-mechanical beam steering device [1], Fresnel lens [2], mirrorless laser [3,4], and adaptive optical components [5,6] etc, in addition to fully successful application to LC displays. However, realization of flexible LC devices, is hardly feasible as LC molecules with fluidity flow under strain induced by mechanical bending force [7,8]. Realization of flexible LC device is also hindered by few technical challenges like difficulty in maintaining uniform cell gap and substrates detachments [9,10]. A super-flexible LC device that is feasible for fabrication of wearable devices is growing interest in recent days because it can be utilized in not only displays but also photonic devices with free form factors, lightweight and wearables [11,12]. A photonic device with flexible diffractive element that allows free-spectral range tunability of light has many potential applications such as hyperspectral imaging, pulsed lasers, wavelength-division-multiplexing, and biomedical imaging where the narrow spectral bandwidth is a big obstacle [13–19]. Even though few approaches are well developed for visible light manipulation like spatial light modulator, surface relief grating, and waveguide/fiber gratings, those do neither support flexible substrates nor utilizes finite spectra bandwidth operations [16,20–22]. Moreover, those are limited by the low efficiency and additional steps in synthesis. The theoretical maximum diffraction efficiency of sinusoidal phase grating is 33.8% [23]. A highly flexible and polarization independent broadband

#379950 https://doi.org/10.1364/OE.27.034876
Journal © 2019 Received 9 Oct 2019; revised 6 Nov 2019; accepted 6 Nov 2019; published 13 Nov 2019

Optics EXPRESS

spectral controlling technique having applications potential in broadband imaging systems is required to be developed.

The nano-structured polymer dispersed LC (nano-PDLC) is a promising candidate for flexible device. Since the LC droplets are covered by the polymer walls in all the directions, it sustains mechanical stress and supports higher bending. Besides, it also possesses an optically isotropic phase at voltage-off state, high transparency, free of surface treatment in fabrication, electro-optic hysteresis free, and fast response time. Previous reports demonstrated that the nano-PDLC is capable of acting as flexible diffraction phase grating with support of bending by 60° [24–28]. However, the broadband light control with highly flexible nano-PDLC device is not yet reported. Furthermore, well developed integrated optics and adaptive optics demands flexible broadband diffractor as they are promising candidate for miniaturized spectrometers and wearable photonics.

Here, we have demonstrated a free-form paper-like flexible optically isotropic LC (OILC) diffractive film consisted of nano-phase separated LC droplets with ultra-flexibility and high transparency. Incorporation of elastomeric monomer to the acrylate monomers results in higher flexibility of fabricated films. The prepared film is self-supported free-standing film feasible to higher bending and rolling. In addition, the obtained film shows an excellent stability against organic and inorganic solvents. Further, the proposed diffractive device exhibits application potential as fast response polychromatic light diffractor.

2. Theory

The structure of nano-PDLC that exhibits an OILC phase is schematically shown in Fig. 1. Briefly, the director of each LC droplet having a size few hundred nanometers with respect to neighboring droplets remains uncorrelated i.e. distributed randomly at field-off state so that an incident light in the visible range does not encounter any periodic modulation of refractive index, and thus the light propagates without diffraction, as shown Fig. 1(a) [29,30]. When an inhomogeneous external field is applied to the interdigitated electrodes, the high positive dielectric anisotropic LC molecules in polymer encapsulated droplet tend to undergo elastic deformations to align LC directors along the field direction between electrodes such that the alignment of LC directors periodically changes, which can give rise to phase modulation and diffract the incident light, as shown in Fig. 1(b). Figures 1(c) and 1(d) depicts a schematic of spatial modulation of refractive index across the cell. When the laser beam passes through the OILC at voltage-on state, it experiences a refractive index modulation with periodicity equal to pitch of the cell and thus diffraction is induced by phase grating. The well-known grating equation for incident wavelength λ in a transmission diffraction mode is written as [31], $n\Lambda(\sin\alpha + \sin\beta) = m\lambda$, where α is incident angle, β is diffraction angle, Λ (=$w + l$) is pitch of the grating, n is the refractive index of the medium, and m is diffraction order. For transmission mode, usually, the incident light hits grating surface normal to the plane of grating, then the grating equation becomes $n\Lambda \sin\beta = m\lambda$. However, this equation is wavelength dependent, i.e., the longer wavelength (red light) diffracts with wider diffraction angle and shorter wavelength (blue light) diffracts with narrow diffraction angle. When the plane wave of white-light beam propagates through the periodically electric field induced birefringent nano-PDLC, it diffracts the light in plane parallel to the grating axis, depending on the magnitude of thelocal refractive index modulation it encounters for particular wavelength. More elaborately, the refractive index n in one pitch can be classified into three regions: n_i (1 and 5 above the electrodes), n' (2 and 4 corresponding to electrode edges), and n'' (3 between two electrode strips), as seen in Figs. 1(c) and 1(d). At voltage-off state, all regions have the same isotropic refractive index n_i, which can be defined as $\nu_p n_p + \nu_{lc} n_{avg}$, where ν_p and ν_{lc} are the filling factors of polymer and LC in the composite, n_p and n_{avg} is the refractive index of the polymer and average refractive index of the LC satisfying the condition $n_p < n_{avg}$ [32,33]. Here n_i varies between n_p to n_{avg}. At voltage-on state, LC directors in nano-sized droplets align along the field direction but the field distribution is inhomogeneous as indicated

Optics EXPRESS

in Fig. 1(d) so that the refractive indices becomes n' and n'', *i.e.*, different from n_i, and its magnitude satisfies the condition $n_i<n'<n''$ and $n_i>n'>n''$ when the polarization direction is parallel (parallel mode) and perpendicular (perpendicular mode) to the grating axis, respectively. In other words, the incident light experiences gradient optical path from region 1 to 5, resulting in diffraction by phase grating. Consequently, the electrically tunable light diffraction can be realized by modulating the refractive index.

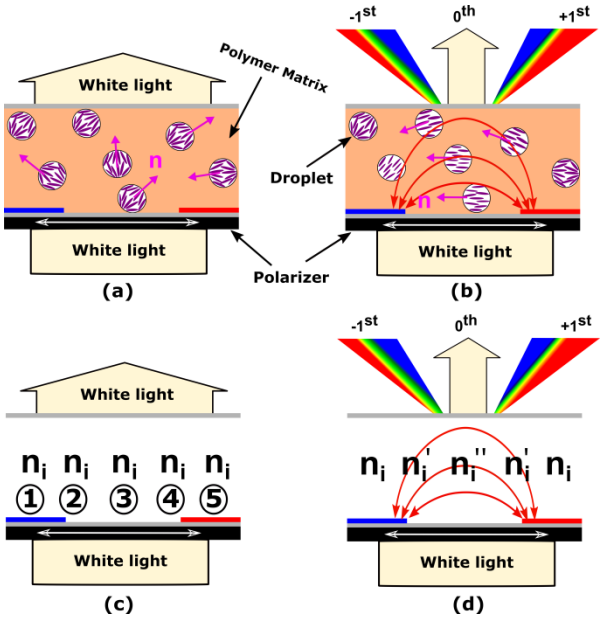

Fig. 1. The structure and driving mechanism of the nano-PDLC at, (a) voltage-off state, and (b) voltage-on state. The schematic of refractive index modulation at voltage-off (c), and voltage-on state (d). n represents the LC director of droplet, n_i is refractive index in the optically isotropic phase, n' and n'' are effective refractive indices at voltage-on state in region 2 & 4 and region 3, respectively. w and l are width and separation of electrodes.

3. Experiments

The flexible nano-PDLC sample consists of nematic LC, MAT-07-1251 (clearing temperature (T_{NI}) = 68 °C, dielectric anisotropy ($\Delta\varepsilon$) = 30.1, birefringence (Δn) = 0.1492, rotational viscosity (γ_1) = 279 mPa·s), and two functionally rich acrylate based monomers, TMPTA (Trimethylol-propane triacrylate) and DPHA (dipentaerythritol penta-/hexa-acrylate), and a silicone elastomer PDMS mixture (Polydimethylsiloxane). The ordinary and extraordinary refractive indices of MAT-07-1251 are n_o=1.4950 and n_e = 1.6442 at 582 nm, respectively. The refractive index (n_p) of TMPTA, DPHA, and PDMS is 1.4740, 1.4830, and 1.40, respectively. The density of TMPTA, DPHA, and PDMS is 1.1 g/mol, 1.15 g/mol, and 0.96 g/mol at 25 °C, respectively. The flow viscosity of TMPTA, DPHA, and PDMS is 80-100 mPa·s, 5000-7000 mPa·s, 3900 mPa·s at 25 °C, respectively. The TMPTA consists of 3 acrylate functional groups at end of the molecular structure while the DPHA consists of 4 acrylate functional groups. The TMPTA appears as transparent liquid and DPHA and PDMS are transparent and high viscous liquids at room temperature. The OILC mixture consists of 40 wt% of MAT-07-1251, 36 wt% of TMPTA, 12 wt% of DPHA, 10 wt% of PDMS, and 2 wt% of Irgacure-907. The PDMS mixture can be synthesized by adding 9 wt% of Sylgard 184A to 1 wt% of Sylgard 184B and mixing thoroughly

Optics EXPRESS

followed by degassing at room temperature to remove the bobbles. The homogeneous mixture of PDMS is added to the homogeneous mixture of LC and monomers and vortex mixing is performed followed by the mechanical mixing methods for 10 min and 1 hr, respectively.

The nano-PDLC film is prepared by spin coating the RMS03-001 (Merck KGaA, Germany) on the glass substrate and followed by a polymerization with UV light. Henceforth, the homogeneous OILC mixture is shear-coated on the RMS03-001 film coated substrate and polymer induced phase-separation was achieved by subsequent UV curing. At this stage, the polymerization of the PDMS is simultaneously achieved by keeping the sample at higher temperature. Finally, another RMS03-001 layer was spin coated on the OILC film and peel-off process was performed.

The OILC phase was identified and characterized by the polarizing optical microscope (POM) (Nikon eclipse E600 POL) attached with a CCD camera (Nikon, DXM 1200). The bulk images of the cell and film was taken by using the digital camera (Samsung, NX1000). The response time of the obtained OILC films is estimated from the voltage dependent-transmittance curves. For electro-optics, we have utilized the interdigited patterned electrodes which consists of uniformly shaped electrodes separated by 4 μm spacing and each electrode width is 4μm. The cell gap was fixed to 10 μm. The efficiency of the dark state calculated from the voltage-off state POM images by using an image analyzer *i*-solution (*i*M Technology, i-Solution Inc.). Finally, the obtained polymer network structures examined by field emission scanning electron microscopy (FESEM).

The diffraction measurements were performed by the collimated white-light. A screen is placed 15 cm behind the test cells to realize the far field diffraction and imaging purposes. The diffraction pattern projected on the screen was recorded with high resolution camera (Samsung, NX1000). The square wave-voltage was applied to the sample by using a function generator (Tektronix, AFG3101C) and amplifier (FLC A400). The efficiency of the diffracted light can be measured by selectively placing the pinhole and the photodiode connected to an oscilloscope (Tektronix, DPO2024B).

4. Results and discussion

4.1. OILC film preparation

The nano-PDLC film preparation process is started by spin coating the mixture of RMS03-001 monomer and a small amount of photo-initiator (1 wt.%) on glass substrate. The coating was prebaked at 100 °C and followed by polymerization with 50 mW/cm^2 intensity UV light for 1 min at 100 °C to realize stable thin film, Figs. 2(a)–2(d). The polymerized RMS03-001 film, hence obtained in firmly stuck to glass substrate. Then, the film was heated to 90 °C and the homogeneous OILC mixture was shear-coated on top of the RMS film. Here, for shear-coating, the LC mixture was poured on the RMS coated substrate and then the mixture was smeared uniformly by mechanically moving the UV blocker. The UV blocker was used as shearing object and at the same time it also protected the rest of the OILC mixture from the UV light, as shown in Figs. 2(e) and 2(f).

The polymerization induced phase-separation of OILC mixture was achieved by irradiating 200 mW/cm^2 intense UV light for 2 min at 90 °C. The substrate was kept for 15 min at same temperature in order to allow PDMS to polymerize. After phase-separation process was done, the substrate was cooled down to room temperature and another layer of RMS03-001 was spin-coated over the PDMS-OILC film followed by the polymerization with 50 mW/cm^2 UV light for 1 min at 100 °C, Figs. 2(g) and 2(h). Finally, the film was peeled-off at room temperature from the substrate after few heating-cooling cycles over T_{NI}, Fig. 2(i). The schematic of the sample preparation was shown in Figs. 2(a)–2(i).

The film produced in above mentioned process is shown in Fig. 3(a). We have been able to fabricate films with its width ~2 cm and length ~3 cm. The clear appearance of text under the film indicates that the obtained film is highly transparent. Figure 3(b) depicts the film under crossed polarizers and the dark indicates the film is optically isotropic, and the light leakage level

Optics EXPRESS

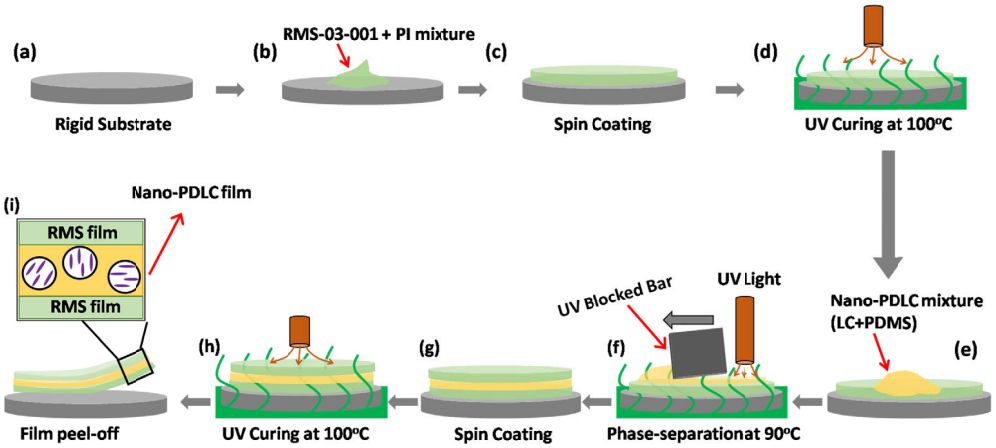

Fig. 2. The schematic of OILC film preparation is shown. RMS layer is coating on glass substrate (a)-(d). Nano-PDLC layer coating and phase-separation depicted (e)-(f). Top RMS layer is coating and UV curing (g)-(h). (i) Peel-off the final film.

presented by numbers in the figures remains about the same, confirming its optical isotropic state before and after peel-off is unaltered. The RMS layer is optically non-birefringent because of its random orientation and unlike acrylate monomers, it weakly adheres to the glass substrate after polymerization. On other hand, it shows an excellent feasibility with acrylate monomers and LC molecules. The RMS layer is intended to use for easy peel-off the nano-PDLC film from glass substrate and, in addition, it also provides a good mechanical and chemical stability after peel-off. Here, the RMS layer plays both roles of protective layer and makes peel-off easier for further processing. In practice, we have experienced that a few heating and cooling cycles of film makes the peel-off easier. The film does not exhibit signatures of damage and degradation during peel-off process. The obtained film can be rolled on a cylindrical surface with diameter ~0.6 cm, as shown in Fig. 3(c). The elastomeric monomer PDMS is aimed to use for improving the flexibility of the film. The PDMS produces a hydrophobic surface which promotes a relatively weak anchored homeotropic orientation of LC molecules at the surface. Since the PDMS usually shows a limited miscibility with LC, a delicate balance between droplet size to decrease light scattering and material concentration is required. In practice, we have also noticed that higher concentration of PDMS damages the film while peeling-off and also reducing efficiency of the optically isotropic nature. The concentration of PDMS employed here is optimized for low light scattering and higher flexibility. Here, transparency and flexibility of the film can also be appreciated from photograph of two times rolled film on the cylinder. The text under the double rolled film still appears clear enough, suggesting high transparency of the prepared film. Appearance of several wrinkles on the film is also evident. It can be presumed that the number of wrinkles can be decreased by adopting laser lift-off method [34]. Small change in film thickness might also cause the formation of wrinkles. The LC droplet's organization for different kind of substrates is shown schematically in Fig. 3(d). Since the droplets are few hundreds of nanometer in diameter and surrounded by the strong polymer walls, the fluidic movement of LC remains highly restricted within the droplets even under external mechanical pressure. Thus the obtained film is not only paper-like flexible, but also self-supported. Even for higher bending like folding, or externally applied pressure the LC configuration in the films remains almost unaltered. However, this approach may need some modification if the substrate itself is flexible, like commercialized flexible displays [35].

Optics EXPRESS

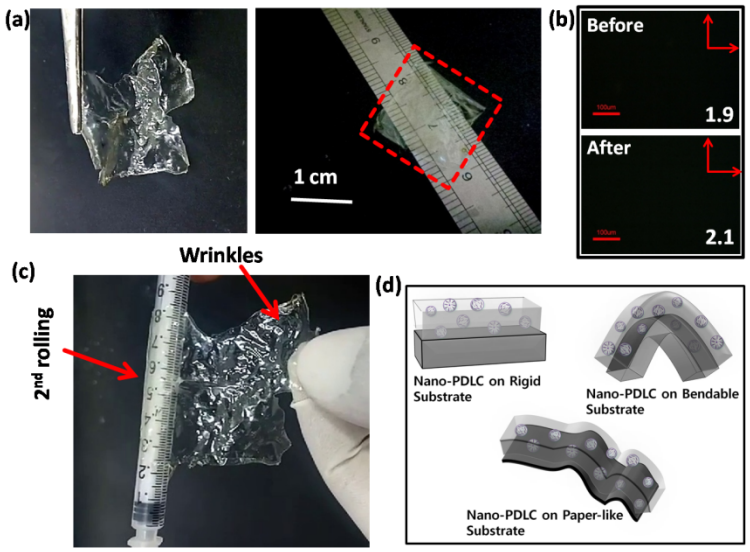

Fig. 3. (a) Synthesized film at ambient light conditions & room temperature. (b) OILC phase observed under crossed polarizers at voltage-off state before and after peel-off. The number depicted on each POM images represents the quantified light leakage under crossed polarizers. (c) Rolled film over cylindrical object. (d) Schematic of structure of Nano-PDLC film on rigid substrate, bending position, and paper-like flexible free standing configuration.

4.2. Optical properties

We have characterized the optical properties of synthesized film by using an UV-Visible spectroscopy. The transmittance of the synthesized films was measured after peel-off from the substrate at room temperature, as depicted in Fig. 4. The film is showing 94% of transmittance at 600 nm which is competitive results in comparison with similar nano-PDLC samples reported elsewhere [24,36]. Slightly reduced transmittance at low wavelengths might be due to feeble light scattering by shorter wavelengths and light absorption of acrylate monomers.

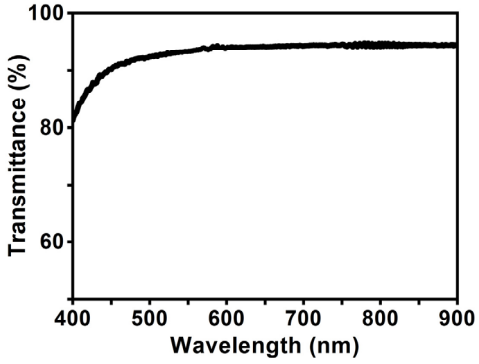

Fig. 4. The wavelength-dependent transmittance of the synthesized film obtained from UV-Visible absorption spectrometer.

Optics EXPRESS

4.3. Switching and response time

The obtained film was characterized with POM. The phase of the film appears dark under crossed polarizers and its darkness remains unchanged on rotation of cell between crossed polarizers, indicating that the achieved phase is optically isotropic. Further, a square-wave voltage was applied to this sample. The sample appears bright due to induced birefringence, as shown in Fig. 5. The rise time is defined as the time taken for rise in transmittance from 10% to 90% whereas decay time is defined as the time taken for change in transmittance from 90% to 10% of its peak value. The measured rise time and decay time are 0.8 ms and 5.4 ms, respectively. The fast rise response is attributed to the smaller droplets of the nano-PDLC. The slow decay time might be due to utilized PDMS which relatively reduces anchoring interaction with LC molecules due to chemical inertness of the PDMS surface after polymerization.

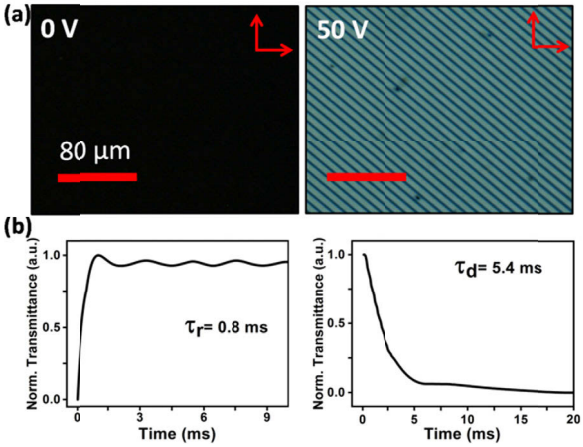

Fig. 5. The switching behavior of prepared OILC film. (a) POM images observed under crossed polarizers at voltage-off (0 V) and voltage-on states (50 V). (b) Measured rise and decay times of prepares nano-PDLC film.

4.4. Chemical stability of the film

We have characterized chemical stability of the film by soaking and washing with various chemicals, Table 1. The soaking characterization was performed by immersing the film into a solution for 10 min. On the other hand, washing was performed by shaking film back and forth deep inside the chemical for 10 min. The final film exhibits a high chemical stability as tested in 10 min soaked film. However, the film was slightly damaged by the chemical while washing. The Nano-PDLC film has shown a good stability against water, acetone, ethanol, and chloroform. However, the film shows less stability against tetrahydrofuran, even very less stability against hexane. It is interesting to notice that the nano-PDLC film is showing high stability against inorganic solvents while exhibiting weak stability with some organic solvents. Furthermore, the obtained film shows a very high stability against humidity. Unlike other LC based films [37,38], this nano-PDLC film is showing a high stability against most of the solvents and humidity. The proposed nano-PDLC film is laminated by RMS film in both sides that improves the chemical stability of the film. After polymerization, the RMS molecules goes through the phase-transition, sudden increase of molecular weight, and limited molecular motions and interactions provides a strong inertness against chemicals and humidity. The thick RMS layers act as protective layers for nano-PDLC films.

Optics EXPRESS

Table 1. Summary of chemical stability characterizations. Here Y: Highly stable; P: Partially stable; N: Not stable.

Solution	Soaking	Washing
Water	Y	Y
Acetone	Y	Y
Ethanol	Y	Y
Tetrahydrofuran	Y	P
Chloroform	Y	Y
Hexane	P	N
Hydrogen Fluoride	Y	Y

4.5. Diffraction measurements

The ability of the film to act as a broadband light diffractor was characterized with the proposed cell. The schematic of the diffraction measurement is shown in Fig. 6(a). We have used unpolarized collimated polychromic light (white-light) as probing beam. The film type polarizer was stuck to the cell's substrate in parallel and perpendicular to the grating axis. The screen was placed behind the sample to capture the diffracted light. The screen can be replaced by the photodiode attached to oscilloscope to measure intensity of diffracted beam and hence to calculate the diffraction efficiency. We have used a pinhole to select and appropriately capture diffracted light beam in photo-detector.

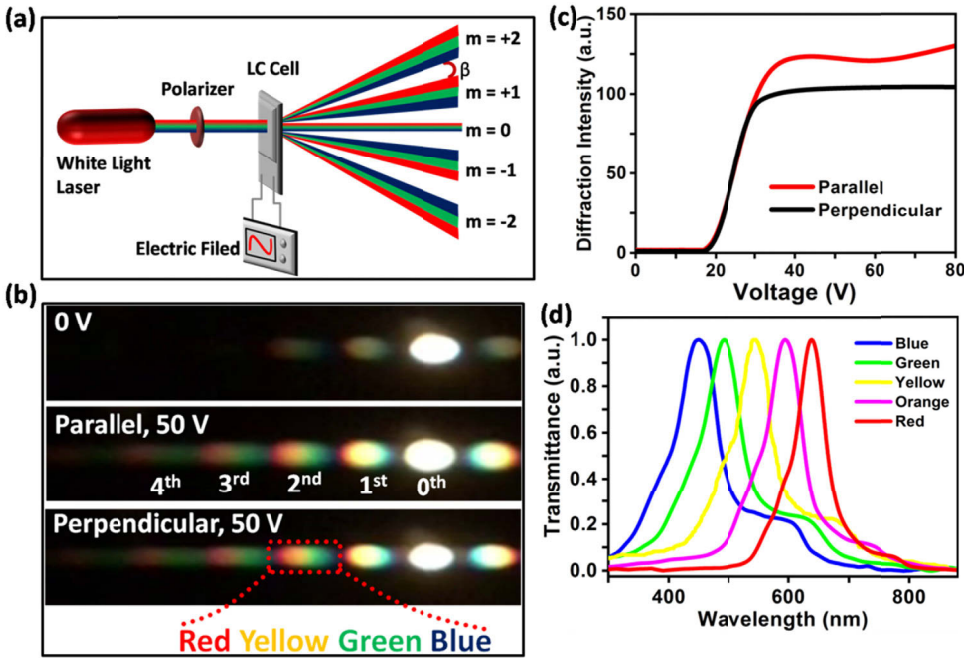

Fig. 6. (a) The schematic of broadband light diffraction of OILC film utilizing inhomogeneous field. (b) Obtained diffraction pattern for parallel and perpendicular modes. (c) Diffraction intensity of 1st order for the parallel and perpendicular modes measured at center of the order. (d) The transmission spectra of 2nd diffraction order parallel polarization.

In voltage-off state, most of the light was focused at zeroth order due to the optically isotropic nature of the film. The inhomogeneous electric field generated by patterned electrodes, makes

Optics EXPRESS

periodic change in refractive index of the film, therefore the transmitted light spatially distributed along the grating axis of the sample. In this case, diffracted light appeared on both sides of the 0^{th} order. As applied field increases, the higher orders become more intense at which Δn_{ind} is saturated for higher voltages. As one can also see from Fig. 6(b), the obtained diffraction is exhibiting wavelength dispersion at every diffraction order. The chromatic dispersion was achieved in diffracted beam. Higher wavelength light is found to take higher angle of diffraction and vice versa. Due to chromatic dispersion, the diffraction spot size increases with increasing number of orders. Since the device is showing a chromatic dispersion, we have selectively chosen a yellow color region within a diffraction spot to estimate the diffraction efficiency. It is interesting to notice that the spatial distribution of the diffracted light intensity is also not uniform. The Fig. 6(b) illustrates the broadband light intensity control as a function of polarization state of the incident light. Since the diffraction phenomena is highly dependent on the polarization direction of the linearly polarized incident light, we have categorized diffraction efficiency for two cases, parallel and perpendicular modes, in which the direction of the plane of polarization is parallel and perpendicular to the grating axis in the former and the latter cases. One can easily notice small difference in diffraction efficiency between parallel and perpendicular modes of polarizations obtained from diffracted beam. Even though there is no spectral shift between parallel and perpendicular modes of polarizations, as shown in Fig. 6(c), the diffraction efficiency is slightly higher for parallel mode. The OILC film exhibits a field induced birefringence after threshold voltage and saturates at operating voltage as well explained by the Kerr effect. The utilized positive dielectric anisotropic LC encapsulated in polymer matrix preferably orients along the field direction i.e. parallel to the grating axis. Hence, induced birefringence experienced by incident beam in parallel mode is higher in comparison with perpendicular mode. Thus the device exhibits higher diffraction efficiency in parallel mode. Fresnel number is defined as [39]; $F = \frac{\Lambda^2}{\lambda R}$ here R is the distance between grating and the screen. R is fixed at 15 cm for our measurements. Calculated Fresnel number is 8.5×10^{-4} which is smaller than one. It clearly indicates that the obtained diffraction belongs to Fraunhofer class that approximates small angle. The Klein factor is defined as [40], $Q = \frac{2\pi\lambda d}{n_{avg}\Lambda^2}$, here d is thickness of the diffractive element, i.e., cell gap. The dimensionless Klein factor Q is 0.3 (<1). Therefore, the obtained grating is Raman-Nath (thin) grating.

We have measured transmission spectra for 2^{nd} order diffraction. The pinhole was used to select certain wavelength and subsequent intensities are measured by spatially shifting the detector and pinhole simultaneously. The obtained data evidences broadband light diffraction covering the wavelength of entire visible range, Fig. 6(d). The bandwidth of the peak is highly sensitive to the spatial selection of the detector. However, the local refractive index modulation of nano-structured LC droplets shows a sharp spectral filtering that makes spectrally selected single color feasible. Further, we have chosen 3^{rd} diffraction order of obtained diffraction pattern and the properties are summarized in the Table 2. The lateral length of 3^{rd} order is measured as 0.9 cm. The diffraction angle (β) was calculated by the grating equation. As one can see from the wavelength dispersive diffraction properties, both spatial frequency and diffraction efficiency are systematically increasing from shorter to longer wavelengths. The paper-like flexible film exhibits an effective diffractive element while possessing the optical isotropic phase and higher transparency.

4.6. Microstructure of the film

Finally, we have characterized polymer network scaffold by using FESEM. The polymer network characterization was done after extracting some of the LC molecules from the sample by keeping the cell in hexane:dichloromethane (80:20) for 3 days. Even though the complete removal of LC molecules from the sample was not possible, the film edges are washed out and used for scanning electron microscope characterizations. We have also observed the edge of the film is

Optics EXPRESS

Table 2. The diffraction properties of 3rd diffraction order.

Colour (wavelength in nm)	Distance from 0th order (mm)	Diffraction angle, β (°)
Blue (460)	41	20.5
Green (530)	42	26.2
Yellow (570)	44	28.4
Red (640)	48	32.3

slightly swollen due to longer soaking in hexane. The cross-sectional surface of the film was sputtered with gold. The images are taken in cross-sectional direction by tilting the substrate at 90°. The cross sectional view of the film under SEM exhibits top and bottom RMS layers and OILC layer all together in a single image. From Fig. 7, it is clear that the highly interlinked bead type polymer network was achieved. Manifestations of thin RMS layers are evident on both sides of the nano-PDLC film. It is evident from Fig. 7 inset, that most of the droplets are smaller than 400 nm. The compatible refractive indices and smaller size droplets are the reasons for high transparency of our OILC film. The obtained OILC film thickness is varying between 12 to 15 μm and the thickness of the bottom and top RMS layers is ~1 μm and ~5 μm, respectively. The small change in film thickness is attributed from mechanically controlled movement of UV block guided by film type spacer during film fabrication.

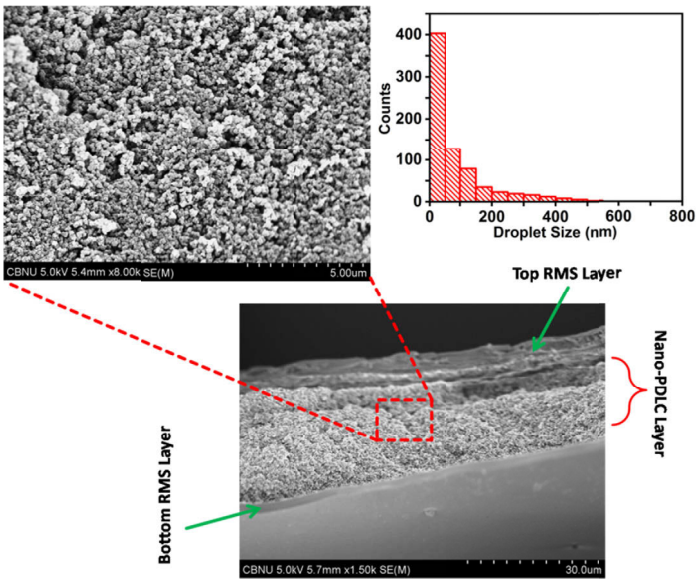

Fig. 7. The FESEM image of prepared nano-PDLC film. Magnified image is shown in inset. The droplet size distribution is also shown in inset.

5. Conclusions

We have demonstrated a paper-like flexible nano-PDLC film which is capable of acting as diffractive element. The obtained film exhibits high transparency and possesses good mechanical stability against small mechanical forces. The proposed optical film has application potential to act as a polychromatic diffractor and the diffraction properties are studied in detail. The film also shows a good chemical stability against both organic and inorganic solvents. In addition, it overcomes the conventional disadvantage of LC devices, while exhibiting an optically isotropic

Optics EXPRESS

phase unchanged. The free-form processability and high flexibility of this isotropic diffractive film has application potential in wearable photonic devices.

Acknowledgments

This research was supported by the Basic Science Research Program through the National Research Foundation of Korea (NRF) funded by the Ministry of Education (2016R1D1A1B01007189) and by the National Research Foundation of Korea (NRF) grant funded the Korea government (MSIT) (No. 2019R1A5A8080326).

Disclosures

The authors declare no conflict of interest.

References

1. J. Stockley and S. Serati, "Advances in liquid crystal beam steering," in *Free-Space Laser Comm. IV* 5550, 32–40 (2004), International Society for Optics and Photonics.
2. S. Sato, A. Sugiyama, and R. Sato, "Variable-focus liquid-crystal Fresnel lens," J. Appl. Phys. **24**(Part 2, No. 8), L626–L628 (1985).
3. H. Coles and S. Morris, "Liquid-crystal lasers," Nat. Photonics **4**(10), 676–685 (2010).
4. T. Matsui, R. Ozaki, K. Funamoto, M. Ozaki, and K. Yoshino, "Flexible mirrorless laser based on a free-standing film of photopolymerized cholesteric liquid crystal," Appl. Phys. Lett. **81**(20), 3741–3743 (2002).
5. J. Arines, "Impact of liquid crystals in active and adaptive optics," Materials **2**(2), 549–561 (2009).
6. E. Oton, J. Perez-Fernandez, D. Lopez-Molina, X. Quintana, J. M. Oton, and M. A. Geday, "Reliability of liquid crystals in space photonics," IEEE Photonics J. **7**(4), 1–9 (2015).
7. H. Sato, H. Fujikake, H. Kikuchi, T. Kurita, and F. Sato, "Rollable ferroelectric liquid crystal devices monostabilized with molecularly aligned polymer walls and networks," Liq. Cryst. **32**(2), 221–227 (2005).
8. Y. Kim, J. Francl, B. Taheri, and J. L. West, "A method for the formation of polymer walls in liquid crystal/polymer mixtures," Appl. Phys. Lett. **72**(18), 2253–2255 (1998).
9. H. Sato, H. Fujikake, H. Kikuchi, and T. Kurita, "Bending tolerance of ferroelectric liquid crystal with polymer walls fastening plastic substrates," J. Appl. Phys. **42**(Part 2, No. 5A), L476–L478 (2003).
10. Y. Obonai, Y. Shibata, T. Ishinabe, and H. Fujikake, "Foldable Liquid Crystal Devices Using Ultra-Thin Polyimide Substrates and Bonding Polymer Spacers," Trans. Inst. Electron., Inf. Commun. Eng., Sect. E **100**(11), 1039–1042 (2017).
11. A. Ranjkesh and T. H. Yoon, "Fabrication of a Single-Substrate Flexible Thermoresponsive Cholesteric Liquid-Crystal Film with Wavelength Tunability," ACS Appl. Mater. Interfaces **11**(29), 26314–26322 (2019).
12. H. C. Jau, Y. Li, C. C. Li, C. W. Chen, C. T. Wang, H. K. Bisoyi, T. H. Lin, T. J. Bunning, and Q. Li, "Light-driven wide-range nonmechanical beam steering and spectrum scanning based on a self-organized liquid crystal grating enabled by a chiral molecular switch," Adv. Opt. Mater. **3**(2), 166–170 (2015).
13. F. Hamouda, A. Aassime, H. Bertin, P. Gogol, B. Bartenlian, and B. Dagens, "Tunable diffraction grating in flexible substrate by UV-nanoimprint lithography," J. Micromech. Microeng. **27**(2), 025017 (2017).
14. K. Yin, Y. H. Lee, Z. He, and S. T. Wu, "Stretchable, flexible, rollable, and adherable polarization volume grating film," Opt. Express **27**(4), 5814–5823 (2019).
15. C. Oh and M. J. Escuti, "Achromatic diffraction from polarization gratings with high efficiency," Opt. Lett. **33**(20), 2287–2289 (2008).
16. N. Collings, W. A. Crossland, P. J. Ayliffe, D. G. Vass, and I. Underwood, "Evolutionary development of advanced liquid crystal spatial light modulators," Appl. Opt. **28**(22), 4740–4747 (1989).
17. A. Hegyi and J. Martini, "Hyperspectral imaging with a liquid crystal polarization interferometer," Opt. Express **23**(22), 28742–28754 (2015).
18. I. Abdulhalim, R. Moses, and R. Sharon, "Biomedical optical applications of liquid crystal devices," Acta Phys. Pol., A **112**(5), 715–722 (2007).
19. P. C. Lallana, C. Vazquez, J. M. Pena, and R. Vergaz, "Reconfigurable optical multiplexer based on liquid crystals for polymer optical fiber networks," Opto-Electron. Rev. **14**(4), 311–318 (2006).
20. M. H. Kim, J. D. Kim, T. Fukuda, and H. Matsuda, "Alignment control of liquid crystals on surface relief gratings," Liq. Cryst. **27**(12), 1633–1640 (2000).
21. A. Madani, H. Khoshsima, H. Tajalli, and S. Ahmadi, "Experimental study of liquid-crystal alignment on a surface relief grating," Laser Phys. **16**(8), 1197–1201 (2006).
22. B. Lee, Y. Jeong, B. Yang, H. S. Seo, S. Choi, and K. Oh, "Electrically controllable liquid crystal fiber gratings," In *Optical Fiber Communication Conference 2000 (FB2)*. Optical Society of America.
23. R. Magnusson and T. K. Gaylord, "Diffraction efficiencies of thin phase gratings with arbitrary grating shape," J. Opt. Soc. Am. **68**(6), 806–809 (1978).

Optics EXPRESS

24. R. Manda, S. Pagidi, Y. J. Lim, R. He, S. M. Song, J. H. Lee, G. D. Lee, and S. H. Lee, "Self-supported liquid crystal film for flexible display and photonic applications," J. Mol. Liq. **291**, 111314 (2019).
25. N. H. Cho, P. Nayek, J. J. Lee, Y. J. Lim, J. H. Lee, S. H. Lee, H. S. Park, H. J. Lee, and H. S. Kim, "High-performance, in-plane switching liquid crystal device utilizing an optically isotropic liquid crystal blend of nanostructured liquid crystal droplets in a polymer matrix," Mater. Lett. **153**, 136–139 (2015).
26. M. S. Kim, Y. J. Lim, S. Yoon, M. K. Kim, P. Kumar, S. W. Kang, W. S. Kang, G. D. Lee, and S. H. Lee, "Luminance-controlled viewing angle-switchable liquid crystal display using optically isotropic liquid crystal layer," Liq. Cryst. **38**(3), 371–376 (2011).
27. S. Aya, K. V. Le, F. Araoka, K. Ishikawa, and H. Takezoe, "Nanosize-induced optically isotropic nematic phase," Jpn. J. Appl. Phys. **50**(5R), 051703 (2011).
28. N. H. Park, S. C. Noh, P. Nayek, M. H. Lee, M. S. Kim, L. C. Chien, J. H. Lee, B. K. Kim, and S. H. Lee, "Optically isotropic liquid crystal mixtures and their application to high-performance liquid crystal devices," Liq. Cryst. **42**(4), 530–536 (2015).
29. S. Zumer and J. Doane, "Light scattering from a small nematic droplet," Phys. Rev. A **34**(4), 3373–3386 (1986).
30. S. W. Choi, S. I. Yamamoto, T. Iwata, and H. Kikuchi, "Optically isotropic liquid crystal composite incorporating in-plane electric field geometry," J. Phys. D: Appl. Phys. **42**(11), 112002 (2009).
31. L. Menez, I. Zaquine, A. Maruani, and R. Frey, "Bragg thickness criterion for intracavity diffraction gratings," J. Opt. Soc. Am. B **19**(5), 965–972 (2002).
32. Y. J. Lim, J. H. Yoon, H. Yoo, S. M. Song, R. Manda, S. Pagidi, M. H. Lee, J. M. Myoung, and S. H. Lee, "Fast switchable field-induced optical birefringence in highly transparent polymer-liquid crystal composite," Opt. Mater. Express **8**(12), 3698–3707 (2018).
33. S. Pagidi, R. Manda, S. S. Bhattacharyya, S. G. Lee, S. M. Song, Y. J. Lim, J. H. Lee, and S. H. Lee, "Fast Switchable Micro-Lenticular Lens Arrays Using Highly Transparent Nano-Polymer Dispersed Liquid Crystals," Adv. Mater. Interfaces **6**(18), 1900841 (2019).
34. R. Delmdahl, R. Pätzel, J. Brune, R. Senczuk, C. Goßler, R. Moser, M. Kunzer, and U. T. Schwarz, "Line beam processing for laser lift-off of GaN from sapphire," Phys. Status Solidi A **209**(12), 2653–2658 (2012).
35. FlexEnable Limited, "Flexible OLCD" https://www.flexenable.com/technology/flexible-olcd/
36. R. Manda, S. Pagidi, S. S. Bhattacharyya, C. H. Park, Y. J. Lim, J. S. Gwag, and S. H. Lee, "Fast response and transparent optically isotropic liquid crystal diffraction grating," Opt. Express **25**(20), 24033–24043 (2017).
37. D. Y. Kim, K. M. Lee, T. J. White, and K. U. Jeong, "Cholesteric liquid crystal paints: in situ photopolymerization of helicoidally stacked multilayer nanostructures for flexible broadband mirrors," NPG Asia Mater. **10**(11), 1061–1068 (2018).
38. J. W. Shiu, K. C. Lee, C. C. Liang, Y. C. Liao, C. C. Tsai, and J. Chen, "A rugged display: Recent results of flexible cholesteric liquid-crystal displays," J. Soc. Inf. Disp. **17**(10), 811–820 (2009).
39. W. H. Carter, "Focal shift and concept of effective Fresnel number for a Gaussian laser beam," Appl. Opt. **21**(11), 1989–1994 (1982).
40. W. R. Klein and B. D. Cook, "Unified approach to ultrasonic light diffraction," IEEE Trans. Sonics Ultrason. **14**(3), 123–134 (1967).